DR 2811

ORNL/TM-6820

MASTER

Electron Energy Confinement in ELMO Bumpy Torus (EBT)

S. Hiroe
G. R. Haste
R. A. Dandl

OAK RIDGE NATIONAL LABORATORY
OPERATED BY UNION CARBIDE CORPORATION · FOR THE DEPARTMENT OF ENERGY

ORNL/TM-6820
Dist. Category UC-20 f, g

Contract No. W-7405-eng-26

FUSION ENERGY DIVISION

ELECTRON ENERGY CONFINEMENT IN ELMO BUMPY TORUS (EBT)

S. Hiroe
Nagoya University, Nagoya, Japan

G. R. Haste

R. A. Dandl
General Atomic, La Jolla, California

Date Published - June 1979

Prepared by the
OAK RIDGE NATIONAL LABORATORY
Oak Ridge, Tennessee 37830
operated by
UNION CARBIDE CORPORATION
for the
DEPARTMENT OF ENERGY

CONTENTS

ABSTRACT v

I. INTRODUCTION 1

II. SPECTRUM DETERMINATION 2

III. EXPERIMENTAL RESULTS 7

A. Electron temperature and density 7

B. Toroidally stored energy 9

C. Hot electron annulus 10

IV. DISCUSSION 11

V. CONCLUSION 16

ACKNOWLEDGMENTS 16

REFERENCES 17

ABSTRACT

Using a calibrated, solid-state, soft x-ray detector, the electron temperature and density have been measured over a wide range of operating conditions of ELMO Bumpy Torus (EBT). The empirical relations of the temperature or the density to the microwave power and the ambient pressure have been determined. The toroidally stored energy has been observed to increase as the stored energy of the hot electron annulus increases. The energy confinement time has been obtained for various plasma parameters and has been found to agree with the neoclassical theory. The advantages of EBT collisionless scaling for fusion plasma confinement have been noted, i.e., $n_e\tau_E$ increases as $T_e^{1.5}$ in the collisionless regime.

I. INTRODUCTION

The microwave heated ELMO Bumpy Torus (EBT)[1,2] plasma consists of three different components: the surface plasma, the energetic electron annulus, and the toroidal plasma. The surface plasma, located near the cavity wall, is characterized by a low density, a low temperature, and a short confinement time. The energetic electron annulus is near the position where the main heating microwave frequency (18 GHz) corresponds to the second harmonic of the local cyclotron frequency and is characterized by an extremely high perpendicular energy and a long confinement time. The high-beta electron annulus modifies the unfavorable vacuum field and acts to stabilize the toroidal plasma.[3] The toroidal plasma is generated and heated by the fundamental electron cyclotron resonance of high power microwaves. The resonance region is located near the cavity throat and covers the entire cross section of the torus. Additional microwave power (10.6 GHz) is applied to the EBT plasma for profile heating. In EBT-I, the fundamental cyclotron resonance region for the 10.6-GHz microwave is close to the second cyclotron harmonic region for 18 GHz; therefore, the additional microwave power is expected to act as the plasma source for the hot electron annulus.

As is well-known,[1] the global behavior of the toroidal plasma is divided into three different operating modes. The operating mode under high ambient pressure and/or low microwave power is called the C-mode and is characterized by low frequency fluctuations. As the ambient pressure is decreased, the density fluctuations decrease and the plasma becomes macrostable. This mode is called the T-mode. As the ambient

BLANK PAGE

pressure is further decreased, the plasma becomes unstable again and MHD type instabilities are observed. This is said to be the M-mode.

The purpose of this report is to study the electron heating and confinement in the T-mode. Typical plasma parameters in the T-mode are as follows: plasma density n_e is $0.5 \sim 2 \times 10^{12}$ cm^{-3}; electron temperature T_e is 200-600 eV; ion temperature T_i is 40-150 eV; neutral density near the axis is of the order of 10^9 cm^{-3}; and the total impurity density to toroidal density ratio is less than 10^{-3}.

In order to observe the electron temperature T_e and density n_e, the energy distribution of the soft x-ray emission from the EBT plasma is measured. The efficiency of a "windowless," lithium-drifted silicon barrier detector [Si(Li)] is not well-defined over the energy range necessary (0.5-1.5 keV) for measurement of the temperature; therefore, the intensity calibration is a very crucial but difficult consideration.

Section II contains the description of the detector calibration and spectrum analysis techniques. In Sec. III, the experimental results are presented. The controllable parameters of EBT operation are microwave power P_μ and ambient pressure p_o. First we show the plasma parameters n_e and T_e as a function of operating parameters P_μ and p_o. Then we introduce an empirical relation of T_e or n_e to P_μ and p_o.

However, the derived empirical relation is not sufficient for an experimental understanding of EBT transport. The confinement of the EBT plasma has been described using neoclassical transport theory.[4,5,6] The comparison of the experimental results with neoclassical theory is given in Sec. IV. Concluding remarks are given in Sec. V.

II. SPECTRUM DETERMINATION

The soft x-ray spectrum emitted by the EBT plasma is measured using a lithium-drifted silicon barrier detector. The spectrum is complicated by a number of effects which tend to obscure the information desired, that is, the spectrum due to the toro 'al electron distribution. A typical spectrum is shown in Fig. 1. Some of the noteworthy features of this spectrum are the high energy continuum due to the energetic electrons, the presence of impurity lines due to aluminum (1.5 keV) and argon (4.0 keV), the reduction below 1.5 keV due to the decreased efficiency and the increase at low energy due to electronic noise. This section will describe the methods used to deal with these effects.

The lithium-drifted silicon barrier detector is used to determine electron temperatures in the range of several hundred electron volts. For this determination, the most serious effect is the loss of efficiency at low energies, a result of the absorption in the material in front of the detector. To minimize this absorption, a "windowless" detector is used, that is, one which does not have the thin beryllium foil typically used as a vacuum and light seal. Although the elimination of the beryllium window helps reduce the low energy attenuation a great deal, there are other absorbing materials which remain. These include a thin, gold electrical contact on the detector face and the silicon dead layer. Also, a very thin foil (carbon and aluminum have been used) serves to reduce the light which strikes the detector. Perhaps the most serious contribution is a result of the gases which

condense on the liquid-nitrogen-cooled detector. The principal component of these gases is water vapor.

It is evident from Fig. 1 that the efficiency calibration is essential to the interpretation of the soft x-ray data. The most believable calibration technique involves the use of x-ray line emitters of known strength, either radioactive sources[7,8,9] or electron excitation of characteristic lines.[10] Although confidence in the calibrations obtained with these techniques is high, it is difficult to use them on-line. Because the condensible gas problem is one which changes with time, it is essential to be able to calibrate the detector in place periodically. The technique used on EBT makes use of the high energy electron component to accomplish this calibration.

For the sake of simplicity, the description of the calibration technique in this section ignores the presence of impurity lines in the spectrum. The differences caused by these lines are easily taken into account.

Free-free bremsstrahlung radiation from a Maxwellian distribution has a spectrum given by[11]

$$I(\varepsilon)d\varepsilon = Gn_e n_i Z_i^2 T_e^{-1/2} \exp(-\varepsilon/T_e)\, d\varepsilon, \qquad (1)$$

where ε is the x-ray energy, G is a geometrical factor, n_e and n_i are the electron and ion densities, respectively, and T_e is the electron temperature.

If the plasma has more than a one-component electron distribution, the spectrum emitted will be a sum of terms with different temperatures. In EBT these terms consist of a contribution from the energetic

electrons with a temperature of ∿100 keV and one from the bulk distribution with a temperature of several hundred electron volts. By varying the magnetic field and microwave power distribution, one or the other of these components may be emphasized.

The high energy component can be emphasized by operating in a mirror mode. This is accomplished by supplying current to two adjacent coils and by supplying microwave power only to the cavity between those two coils. In that case, there is no toroidal confinement and the low energy component is negligible.

The bremsstrahlung spectrum is then due to the high energy electrons, and this spectrum is assumed to be known. Because the detector efficiency above ∿3 keV is unity, the assumed spectrum is made to fit the measured one in that region. Next, the assumed spectrum is extrapolated down to low energies. The detector efficiency is then the ratio of the measured spectrum to the extrapolation. This method automatically results in an efficiency of unity at high energy (that is, above 3 keV). The efficiency at low energy falls as expected from the window absorption. Figure 2 shows this procedure. The solid points are the experimental points, the line through those points is the assumed spectrum, and the open circles are the reciprocal of the detector efficiency.

In contrast to this calibration procedure, where the energetic component is maximized, the data for the toroidally trapped distribution are taken with this high energy component minimized. This minimization is achieved by eliminating the microwave power feed to that cavity seen by the detector. The measured spectrum is then corrected by dividing by the efficiency curve. The high energy portion

of the spectrum, which is due to the residual energetic electron distribution, is fit by a straight line on the semilog plot, and this assumed component is subtracted from the corrected spectrum. The remaining spectrum is then that due to the toroidally trapped electrons. Figure 3 shows two of these spectra, fit with lines corresponding to 210- and 320-eV plasmas.

The technique described above ignores the contributions due to impurity lines. In practice, one is forced to eliminate from the analysis the spectral regions occupied by these lines. For this reason, a detector with good resolution is desirable so as to eliminate as little of the spectrum as possible.

III. EXPERIMENTAL RESULTS

A. Electron temperature and density

The electron temperatures obtained by the method described above are plotted in Fig. 4 against the ambient pressure with microwave power as a parameter. It is evident that the electron temperature increases as the ambient pressure decreases and/or as the microwave power increases. Lower temperatures are obtained with profile heating than without profile heating. As is now known, the toroidally stored energy with profile heating is higher than that without profile heating.

The line density from the 70-GHz interferometer does not distinguish the surface plasma from the toroidal plasma. The density measured by the soft x-rays, on the other hand, is clearly the toroidal density because the contribution to bremsstrahlung radiation from the cold surface plasma is negligibly small, in the energy range of 0.5-1.3 keV.

The density from the soft x-ray measurement decreases as the ambient pressure increases. However, the density from the 70-GHz interferometer is an increasing function of the ambient pressure. A reasonable explanation for the above difference is that the surface plasma density is an increasing function of the ambient pressure. In these experiments, the density from the soft x-ray measurements was normalized to the density of the interferometer measurement at a low ambient pressure operating condition where the contribution of the surface plasma to the interferometer measurement is negligibly small. It is meaningful to point out that the density from the soft x-ray measurement is contributed from the higher temperature region, that is, near the axis.

In Fig. 4 the toroidal densities with and without profile heating are plotted as a function of the ambient pressure with the microwave power as a parameter. It is interesting to note that, in the case without profile heating, the toroidal density increases as the ambient pressure decreases and as the microwave power increases. For the profile heating case, the toroidal density first increases and then decreases as the ambient pressure increases. A higher input power generates a higher density plasma. Note also that a higher density is sustained with profile heating than without profile heating.

The empirical relations among T_e, n_e, P_μ, and p_o for the case without profile heating are shown in Fig. 5. Most of the data are represented by the following simple relations:

$$T_e \propto P_\mu^{1/2}/p_o \tag{2}$$

$$n_e \propto P_\mu^{3/2}/p_o \quad . \tag{3}$$

For the case with profile heating, the empirical relation for electron temperature is almost the same as Eq. (2), but the empirical relation for density is not as simple as Eq. (3).

B. Toroidally stored energy

Equations (2) and (3) indicate that the toroidally stored energy is described by

$$\frac{3}{2} n_e kT_e \propto (P_\mu/p_o)^2 \quad . \tag{4}$$

Higher stored energy is obtained as the microwave power increases and the ambient pressure decreases. This dependence is shown in Fig. 6. It is clear that the dependence on P_μ/p_o is different for the cases with and without profile heating. (At the present time we are unable to explain this difference clearly.) However, it is encouraging that the stored energy increases as P_μ/p_o is increased.

In early EBT experiments,[1] empirical relations were found between microwave power and ambient pressure defining the transition from C-mode to T-mode. The relation for the C-T transition was roughly written by

$$p_o(\text{torr}) \sim 10^{-6} P_\mu^{0.5} \quad (P_\mu \text{ in kW}) \quad . \tag{5}$$

In this case, Eq. (4) can be rewritten as

$$\frac{3}{2} (nkT_e)_{C\text{-}T} \sim P_\mu \quad . \tag{6}$$

The stored energy at the C-T transition increases in proportion to the input microwave power.

C. Hot electron annulus

The diamagnetism of energetic electron annulus produced by electron cyclotron heating modifies the unfavorable magnetic curvature and, as a result, stabilizes the toroidal plasma. The correlation between the toroidally stored energy and the energy deposited in the annulus is examined next.

The plasma parameters of the hot electron annulus change with the ambient pressure in the same manner as the toroidal plasma, as shown in Secs. III.A and III.B. As the ambient pressure is decreased or as the microwave power is increased, the hot electron temperature and density are observed to increase, and the perpendicular energy $W_\perp$ measured with the diamagnetic loop increases also. So a better toroidal plasma is supported by a more energetic annulus. This is shown in Fig. 7.

A comparison of the toroidally stored energy for the cases with and without profile heating reveals no difference in the higher stored energy regime. However, for a smaller value of stored energy of the annulus, the toroidally deposited power with profile heating is larger than that without profile heating. As the operating mode is varied from the C-T transition to the T-M transition, the toroidally and annularly deposited powers increase.

This result can be correlated to the fluctuation level and the annularly deposited energy as reported in Ref. 1. At a value of annularly deposited energy lower than that at the C-T transition (C-mode), no gross instabilities are seen, but density fluctuations are observed in frequency ranges suggestive of drift waves. As the annular energy increases, the fluctuation level drops to very low values (T-mode).

When the annular energy increases beyond the T-M transition, MHD type instabilities are observed. It is significant that the toroidally deposited power increases as the fluctuation level decreases.

IV. DISCUSSION

Transport in bumpy torus type geometries has been investigated by several authors.[4,5,6] Kovrizhnykh[6] applied neoclassical theory to compute analytic expressions for particle and energy fluxes across magnetic fields in various toroidal magnetic systems. For the bumpy torus, Kovrizhnykh considered only the limit of very large radial electric fields where the results, in general, do not depend on the poloidal component of the electric field. Spong et al.[5] have obtained the numerical value of the radial diffusion coefficient for finite radial electric fields.

For the present plasma parameters of EBT, the main electron energy loss of the toroidal plasma is diffusive; therefore, the energy transfer from electrons to ions, the ionization loss, etc. can be neglected. Then the electron energy balance equation becomes

$$\frac{\alpha P_{\mu}}{V} = \frac{3/2\ nkT_e}{\tau_E} \quad , \tag{7}$$

where τ_E is the electron energy confinement time, V is the total cavity volume, and α is the fraction of the microwave power absorbed in the toroidal plasma.

When the energy loss is neoclassical, the energy confinement time is given by

$$\tau_E^{-1} = \frac{V_o^2}{2\Omega}\left(\frac{2.405}{a}\right)^2 [K_n' (1 + e\phi/kT_e) + K_T'] \quad , \tag{8}$$

where $V_o = 2kT_e/eBR$, B is the magnetic field strength, a is the plasma radius (10 cm), R is the major radius (150 cm), Ω is the poloidal drift frequency, ϕ is the ambipolar potential, and K_n' and K_T' are the normalized heat transfer coefficients.

The detailed calculation of the transport coefficients K_n' and K_T' was carried out by D. A. Spong et al.[5] by using the bounce-averaged poloidal drift frequency, which is given by

$$\nu/\Omega = \frac{\nu}{kT_e/eB_rR_c}\left(1 + 0.7\,\frac{e\phi}{kT_e}\right)^{-1} \quad , \tag{9}$$

where R_c is a radius of curvature of poloidal magnetic field, ν is a collision frequency, and ϕ is an ambipolar potential. In the case considered by Kovrizhnykh, these coefficients are a simple function of collisionality ν/Ω. Then Eq. (8) is written by

$$\tau_E = \text{const}\ A^2\,\frac{B}{T_e}\left(\frac{(\nu/\Omega)}{1 + (\nu/\Omega)^2}\right)^{-1} \quad , \tag{10}$$

where A is the aspect ratio. It is interesting that τ_E increases as the aspect ratio and magnetic field increase.

From Eq. (10) $T_e\tau_E$ is easily seen to be a simple function of ν/Ω. In the collisionless regime, $T_e\tau_E$ is a decreasing function of collisionality. When ν/Ω exceeds one, $T_e\tau_E$ becomes an increasing function of ν/Ω.

The experimental plots shown in Sec. III are displayed as a function of experimentally controllable parameters, e.g., the microwave input power and ambient pressure. Comparison of experiments with transport theory is facilitated by use of collisionality as a parameter.

Figure 8 is a plot of the relation between collisionality and ambient pressure with microwave power as a parameter. Collisionality is an increasing function of ambient pressure. At low pressures, collisionality is almost independent of power with and without profile heating, but the plasma with profile heating is more collisional than the plasma without profile heating. As the ambient pressure increases, collisionality rises to a peak the height of which depends on microwave power. The region at higher ambient pressure than the pressure at the peak is referred to as the C-T transition. These points correspond to the data near the straight line in Fig. 4.

In Figs. 9 and 10, the electron temperature and density are plotted against collisionality with microwave power as a parameter. The temperature decreases monotonically as the collisionality increases. The density, however, is high for both low and high collisionality. As expected the experimental results do not strongly or systematically depend on the microwave power, depending instead on collisionality. This indicates that collisionality is the important parameter for understanding the heating and confinement of EBT plasma.

In Fig. 11 the experimental values of $T_e\tau_E$ are compared with the neoclassical energy confinement time.[9] It is very difficult to determine the exact energy confinement time experimentally because it is necessary to measure the microwave absorption rate by the surface plasma, the electron annulus, and the toroidal plasma separately for each operating condition. As a rough estimate, the hot electron annulus absorbs $\sim$25% of the microwave power, and the absorption rate of the surface plasma is 25%. Therefore, the absorption rate of the toroidal plasma must be

$\sim$50%. In this experiment, the microwave power P_μ is the output power of the microwave tube. The loss from the tube to the cavity is $\sim$35%. The best estimate of the absorption fraction for the toroidal plasma is 25-40%. In order to calculate the energy confinement time, this fraction is assumed to be constant and to be $\sim$30%.

It appears from Fig. 11 that as the collisionality increases, $T_e\tau_E$ decreases to a constant. The spread of data points comes from the different operating modes.

The theoretical curves (solid line) in Fig. 11 are shown with $e\phi/kT_e$ as a parameter. In this experiment, this ratio has been measured and found to range from 0.25-0.7. When the experimental data are compared with the theoretical prediction, it is found that the curve which best fits the experimental data corresponds to a higher potential than the measured value. Except for this relatively small difference, the EBT plasma follows neoclassical transport theory.

In Sec. III, it was shown that higher energy annuli sustain plasmas with greater toroidally deposited energy because the annulus confines the toroidal plasma stably by the favorable modification of the magnetic curvature. This modification of the magnetic curvature not only stabilizes the toroidal plasma but also increases the poloidal drift frequency because of the decrement of R_c in Eq. (9). Increasing the poloidal drift frequency decreases the collisionality and increases the confinement time. This is suggested in Fig. 11, where the subscripts of the data points indicate the relative value of the annularly stored energy. A larger value of the annularly stored energy corresponds to better

confinement. This is shown more clearly in Fig. 12, where $T_e\tau_E$ is plotted against the annularly deposited energy with collisionality as a parameter. When the collisionality is kept constant and $W_\perp$ increases, $T_e\tau_E$ is observed to increase. Thus, lower collisionality and larger annularly stored energy support higher temperature and better confined EBT plasmas. Note that this better confined EBT plasma corresponds to the T-M transition. Thus, EBT operation under high microwave power and low ambient pressure sustains the best plasma. However, when EBT is operated at lower pressure below the T-M transition, macroinstabilities are observed.

From the fusion point of view, it is important to consider the relation between $n\tau_E$ and T_e. The experimental data points of $n\tau_E$ are plotted in Fig. 13 with density as a parameter. For the case of low density, $n\tau_E$ increases as the temperature increases. In the high density regime, $n\tau_E$ is also observed to increase as T_e increases. Qualitatively, this feature is easily understood from Eq. (10). The dependence of $n\tau_E$ on n and T_e is written

$$n\tau_E \sim \begin{cases} T_e^{1.5} & \text{in the collisionless region} \\ n^2\, T_e^{-3.5} & \text{in the collisional region} \end{cases} . \qquad (11)$$

In the collisionless regime, $n\tau_E$ depends only on $T_e^{1.5}$. On the other hand, the value of $n\tau_E$ in the collisional region depends on the square of density and varies as $T_e^{-3.5}$.

V. CONCLUSION

The measurements of the electron parameters described above have been made with a soft x-ray detector which has been calibrated in place, and which is sensitive to the toroidally confined component as well as the energetic ring component. The following conclusions apply to the toroidally confined component:

1) The electron temperature increases as the ambient neutral pressure decreases. Higher temperatures are observed as the microwave power increases.

2) The electron density without profile heating decreases as the ambient pressure decreases. The density with profile heating has a maximum at some pressure. The observed densities without profile heating are systematically lower under these conditions than with profile heating.

3) The toroidally stored energy is an increasing function of P_μ/p_o.

4) The toroidally stored energy is found to increase as the power deposited in the annular increases.

5) EBT electron transport is collisionless neoclassical. In the collisionless neoclassical regime, $n\tau_E$ rises as the temperature increases, e.g., $T_e^{1.5}$. This region is very attractive from a reactor point of view.

ACKNOWLEDGMENTS

The authors would like to express their appreciation to the EBT experimental and theoretical staff members for many helpful discussions. One of the authors, S. Hiroe, would like to acknowledge the continuing encouragement of K. Takayama and H. Ikegami, professors at the Institute of Plasma Physics, Nagoya University, Nagoya, Japan.

REFERENCES

[1]R. A. Dandl, H. O. Eason, G. E. Guest, C. L. Hedrick, H. Ikegami, and D. B. Nelson, in *Plasma Physics and Controlled Nuclear Fusion Research* (International Atomic Energy Agency, Vienna, 1975), Vol. 2, p. 141.

[2]C. L. Hedrick, R. A. Dandl, J. A. Cobble, R. A. Dory, H. O. Eason, E. G. Harris, G. R. Haste, H. Ikegami, E. F. Jaeger, N. H. Lazar, D. H. McNeill, D. J. McAlees, D. B. Nelson, L. W. Owen, D. A. Spong, and N. A. Uckan, in *Plasma Physics and Controlled Nuclear Fusion Research* (International Atomic Energy Agency, Vienna, 1977), Vol. 2, p. 145.

[3]D. B. Nelson and C. L. Hedrick, Oak Ridge National Laboratory Report ORNL/TM-5967 (1977) (to be published in Nucl. Fusion).

[4]E. F. Jaeger, D. A. Spong, and C. L. Hedrick, Phys. Rev. Lett. 40, 866 (1978).

[5]D. A. Spong, E. G. Harris, and C. L. Hedrick (to be published in Nucl. Fusion).

[6]L. M. Kovrizhnykh, Sov. Phys.—JETP 29, 475 (1969).

[7]J. S. Hansen, J. C. McGeorge, D. Nix, W. D. Schmidt-Ott, I. Unus, and R. W. Fink, Nucl. Instrum. Methods 108, 365 (1973).

[8]D. B. Rosner, D. Gur, and L. Shabason, Nucl. Instrum. Methods 131, 81 (1975).

[9]G. Hubricht, B. Kanf, G. Presser, and J. Stahler, Nucl. Instrum. Methods 144, 359 (1977).

[10]C. E. Dick, A. C. Lucas, J. M. Motz, R. C. Placious, and J. H. Sparrow, J. Appl. Phys. 44, 815 (1973).

[11]T. F. Stratton, *Plasma Diagnostic Techniques* (Academic Press, New York, 1965), p. 362.

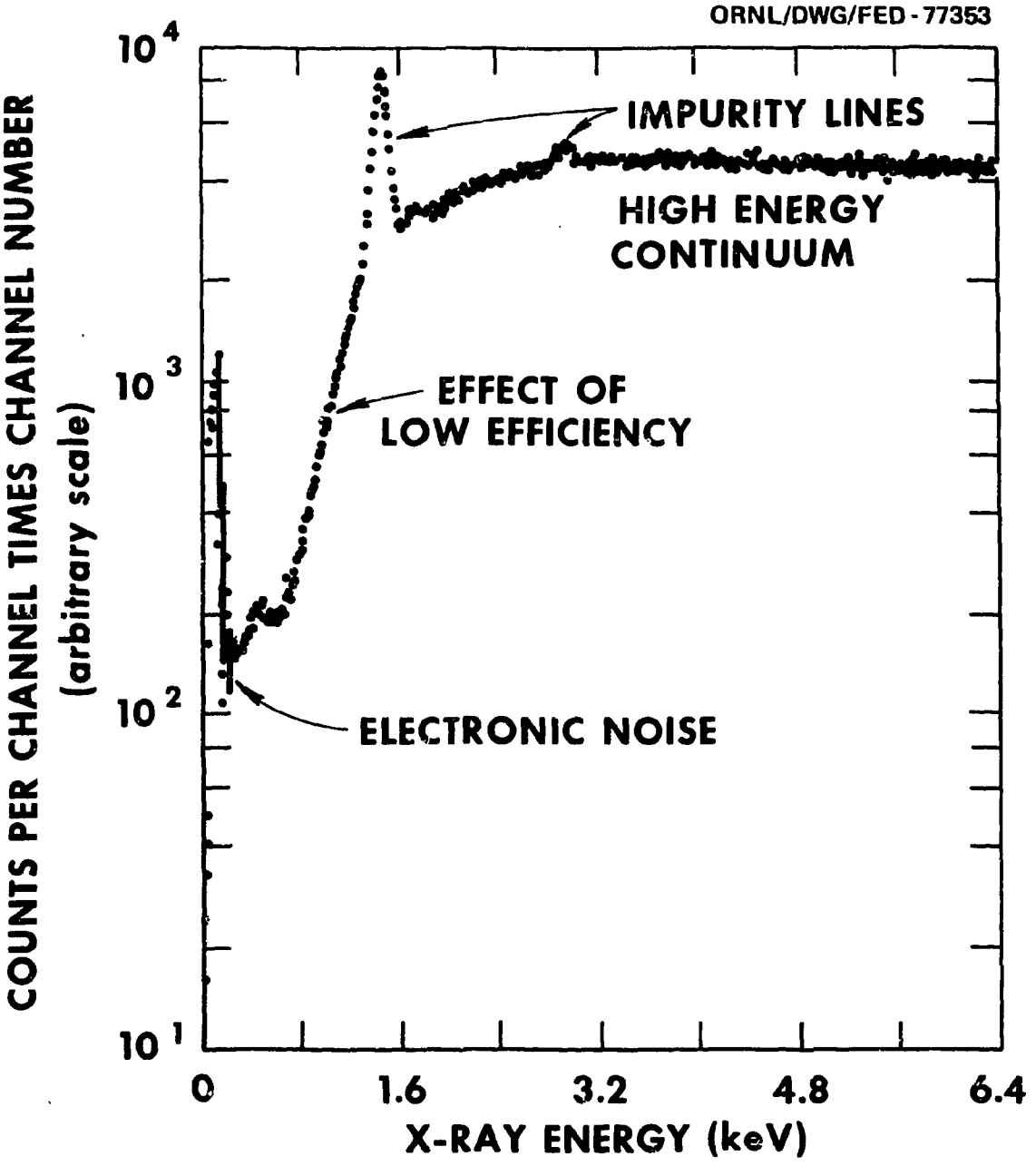

Fig. 1. A typical x-ray spectrum showing the effects of electronic noise, inefficiency at low energy, impurity lines, and the high energy continuum.

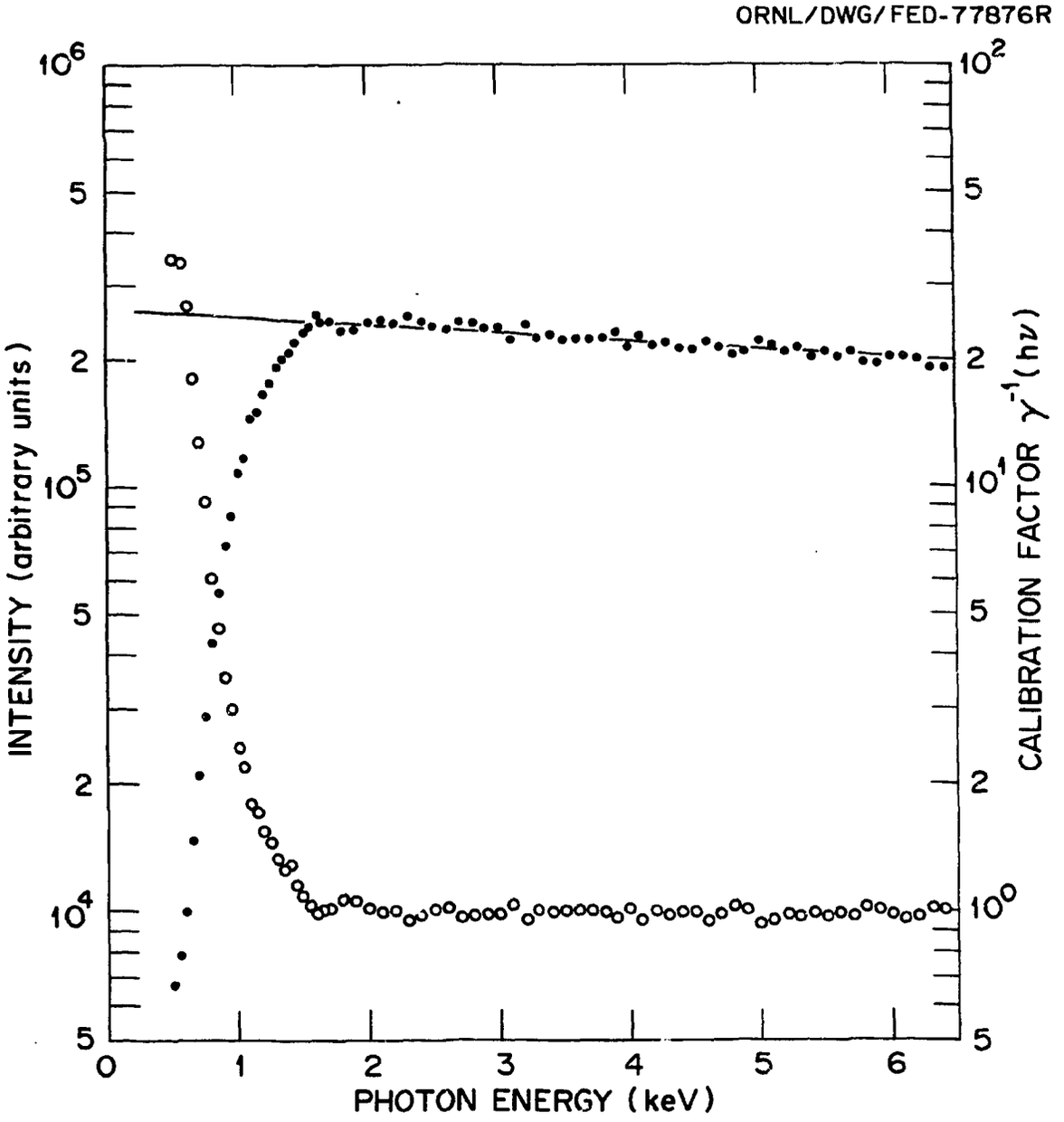

Fig. 2. Calibration procedure. The solid curves are the experimental spectrum, the straight line is a fit to this spectrum, and the open circles are the correction values for the detector efficiency.

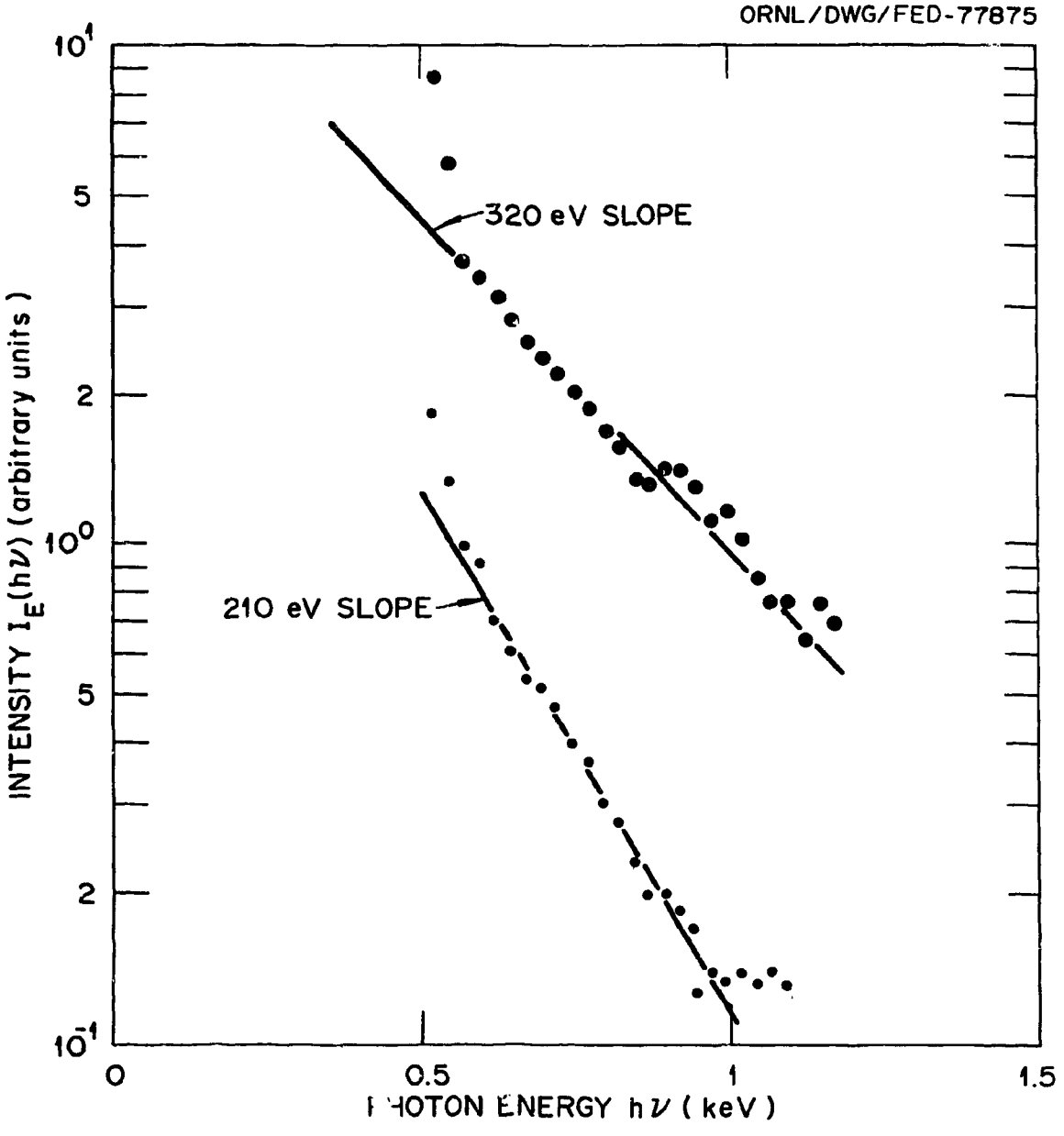

Fig. 3. Typical x-ray spectra due to toroidally trapped electrons.

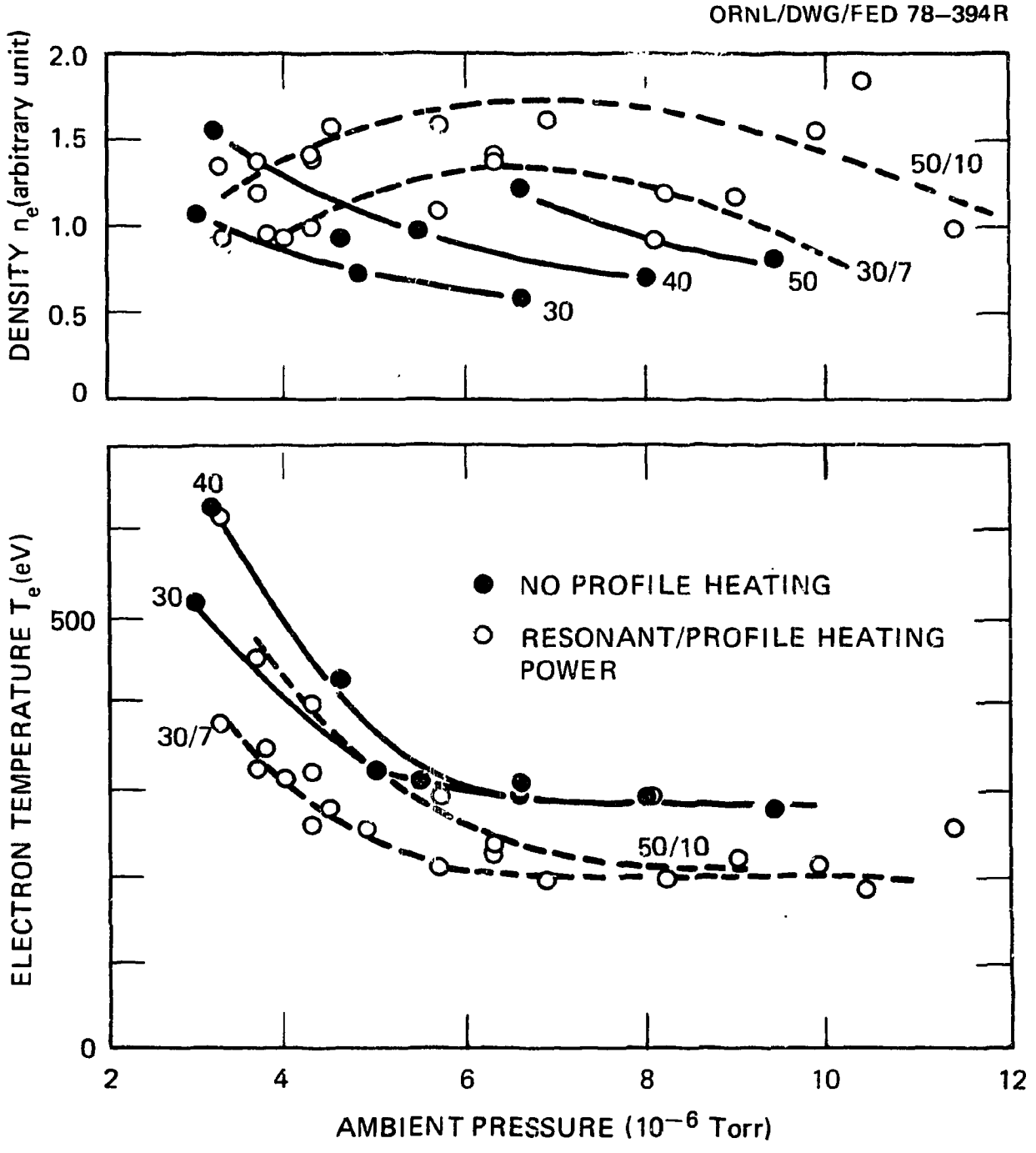

Fig. 4. Electron temperature and densities are plotted against ambient pressure with microwave power as a parameter. The closed circles show the data without profile heating, and the open circles show the data with profile heating. The figures indicate the microwave power used — main power/profile power.

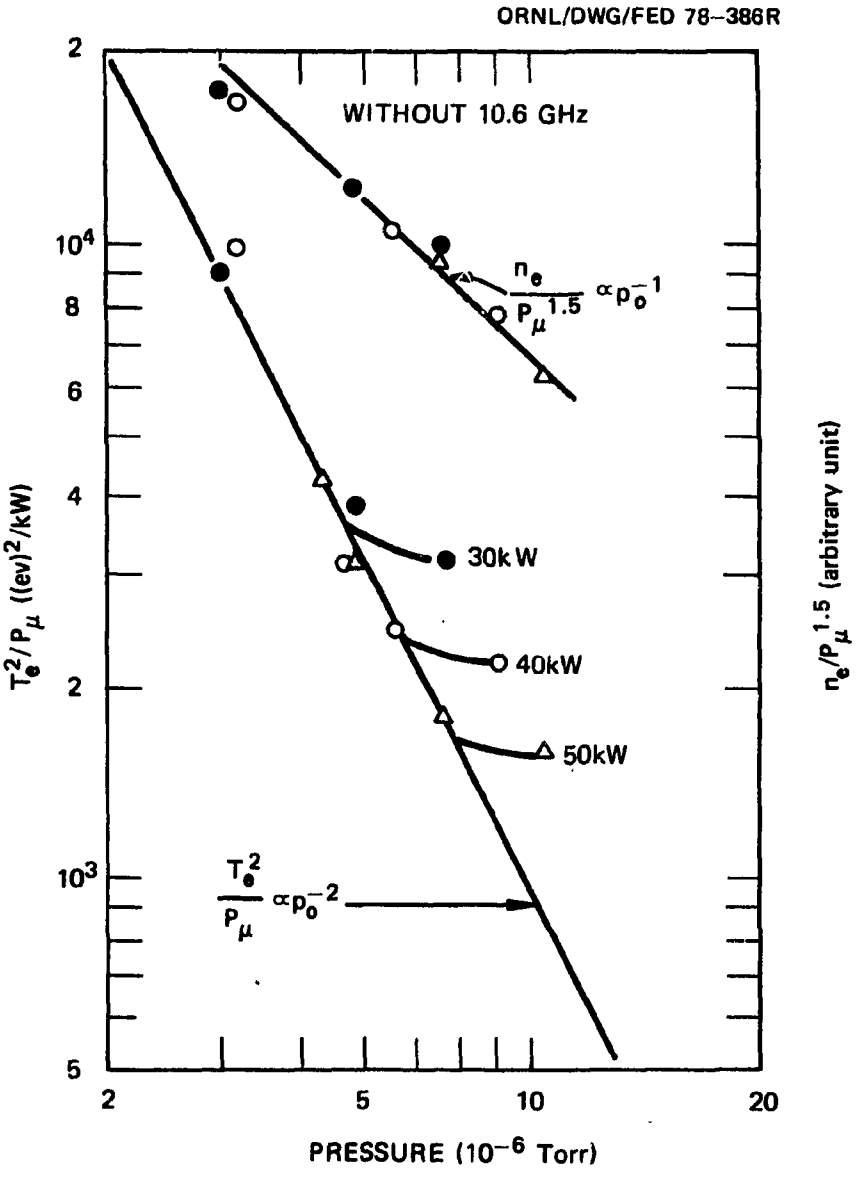

Fig. 5. Plot of temperature and density vs ambient pressure. The solid lines are the empirical relations for the case without profile heating.

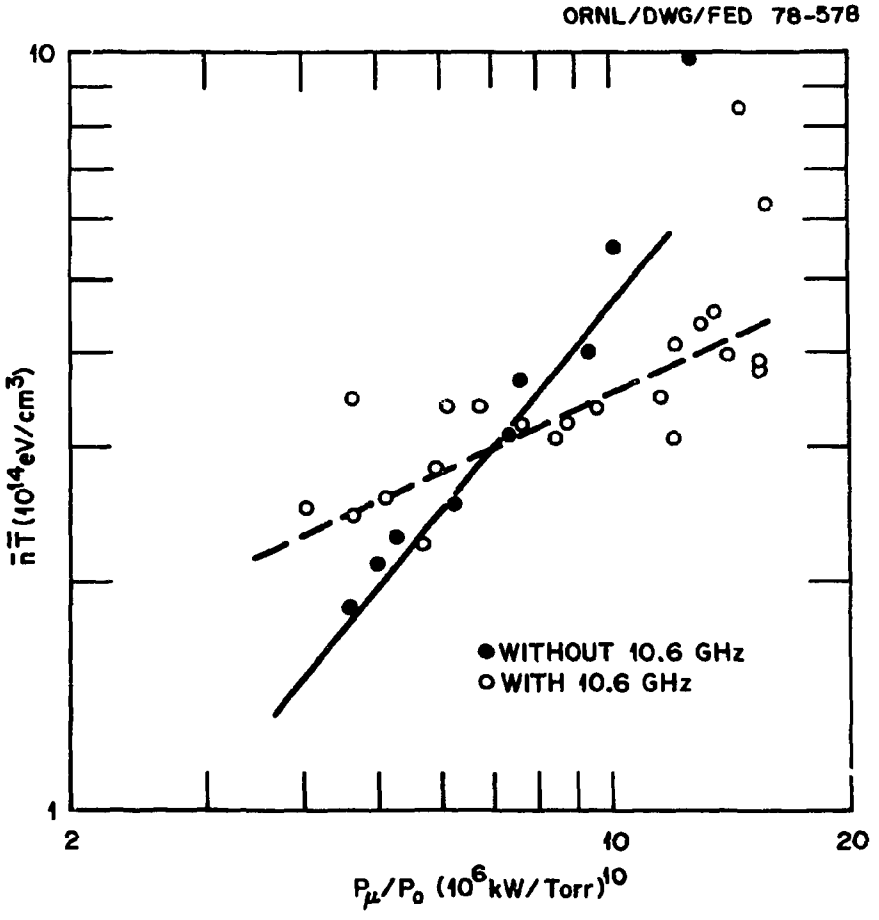

Fig. 6. Toroidally stored energy plotted against the value P_μ/p_o.

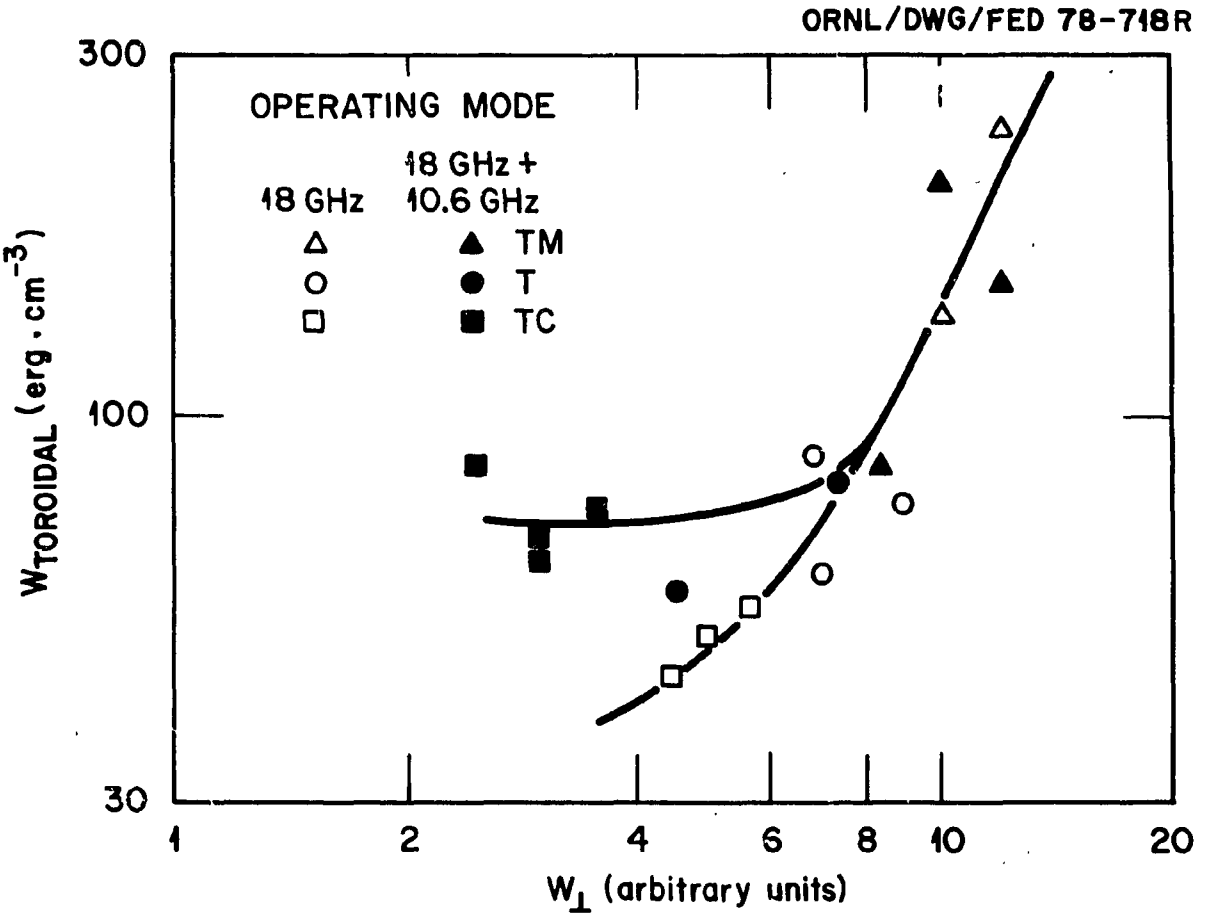

Fig. 7. Correlation of the stored energy of the toroidal plasma and the annulus. Open and solid points show the data without and with profile heating, respectively.

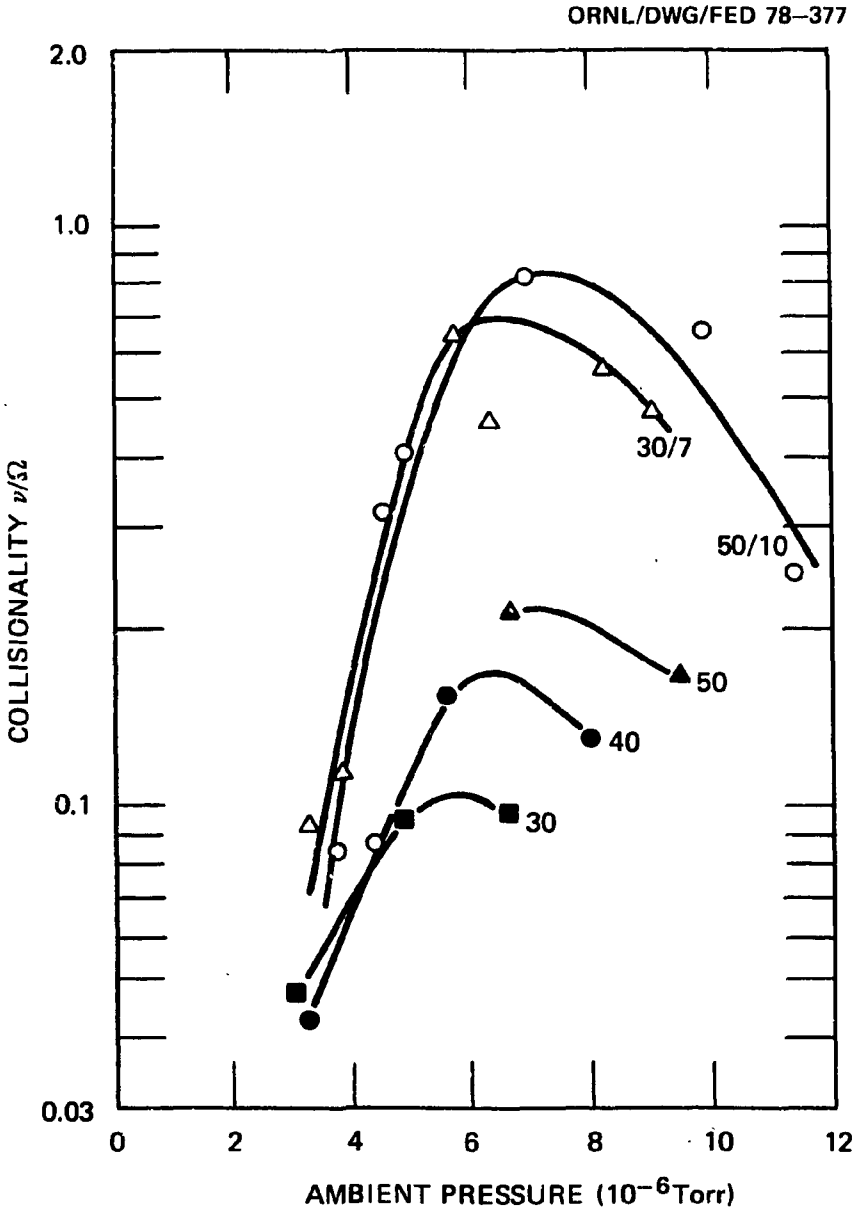

Fig. 8. Collisionality is plotted against ambient pressure with microwave power as a parameter. Open and solid points correspond to the data with and without profile heating, respectively.

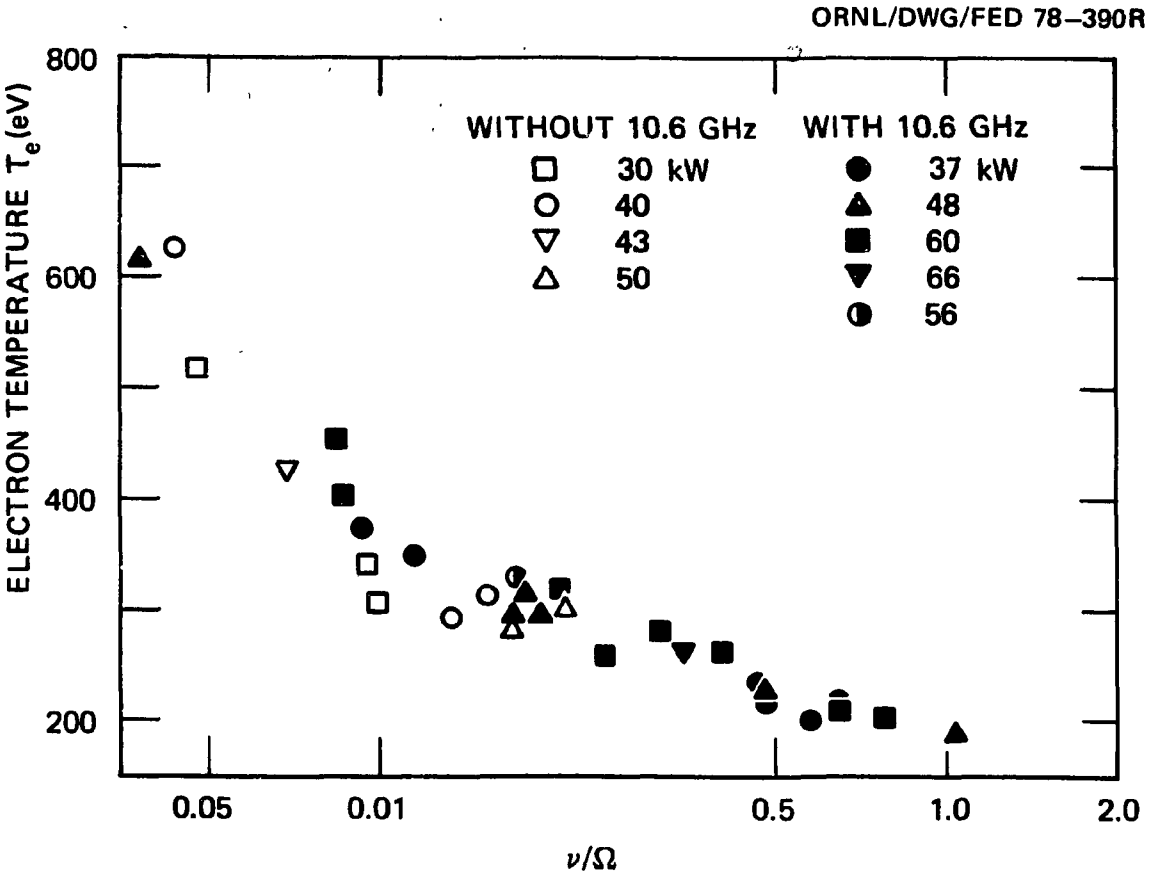

Fig. 9. Electron temperatures plotted against collisionality with total microwave input power as a parameter.

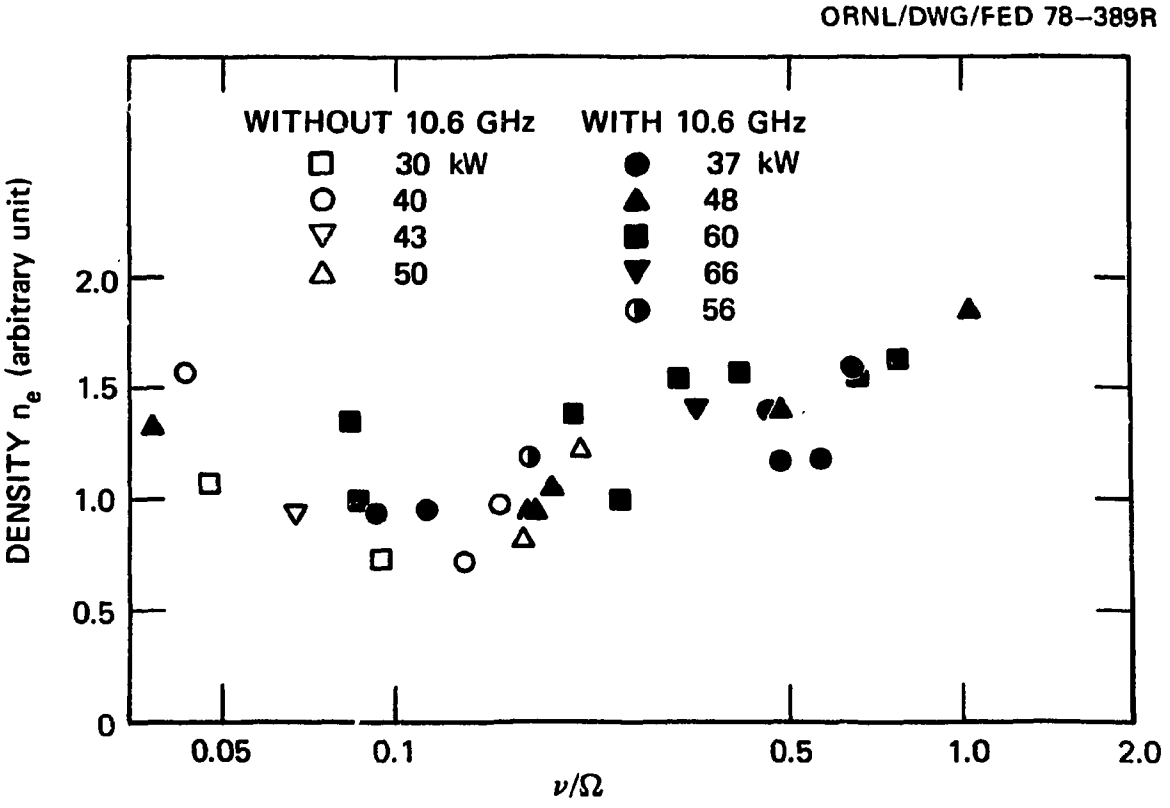

Fig. 10. Electron densities plotted against collisionality with total microwave input power as a parameter.

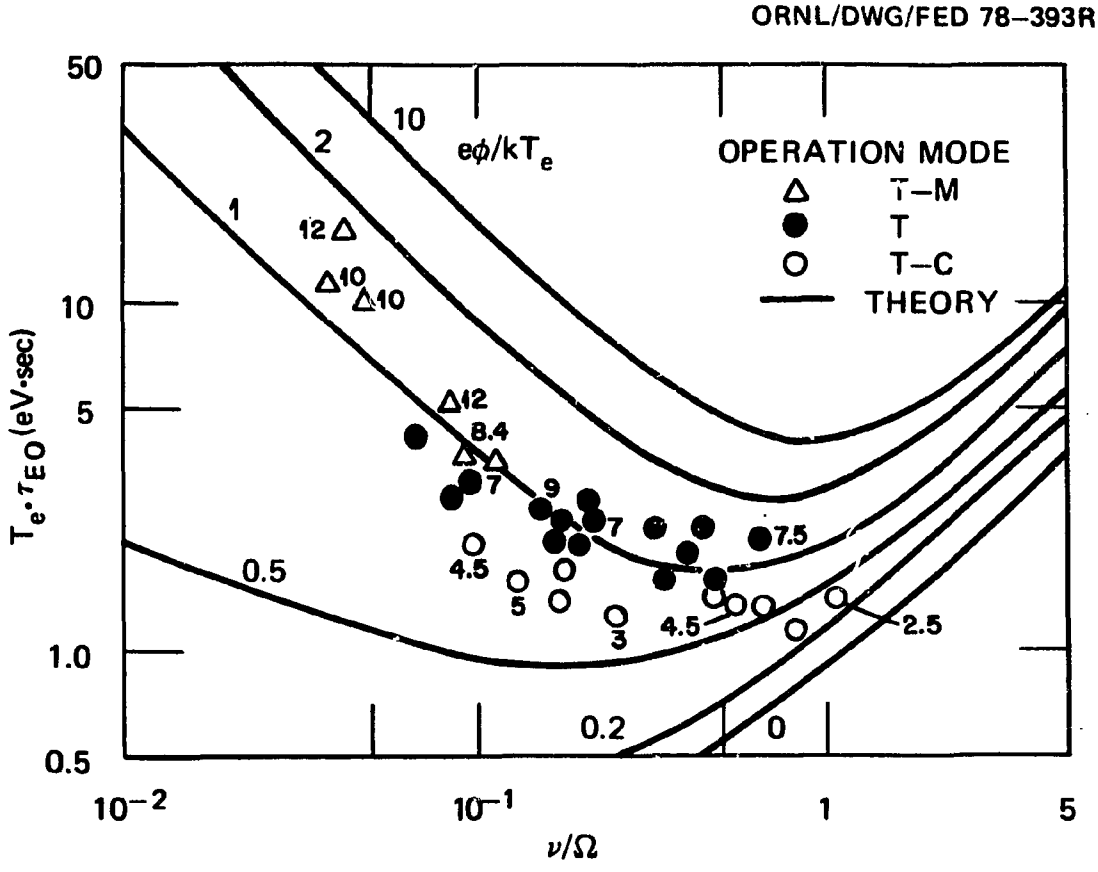

Fig. 11. Normalized energy confinement time obtained experimentally is displayed as a function of collisionality. The theoretical prediction calculated by Spong et al. is shown with $e\phi/kT_e$ as a parameter. The number beside the data points is $W_\perp$ of the annulus.

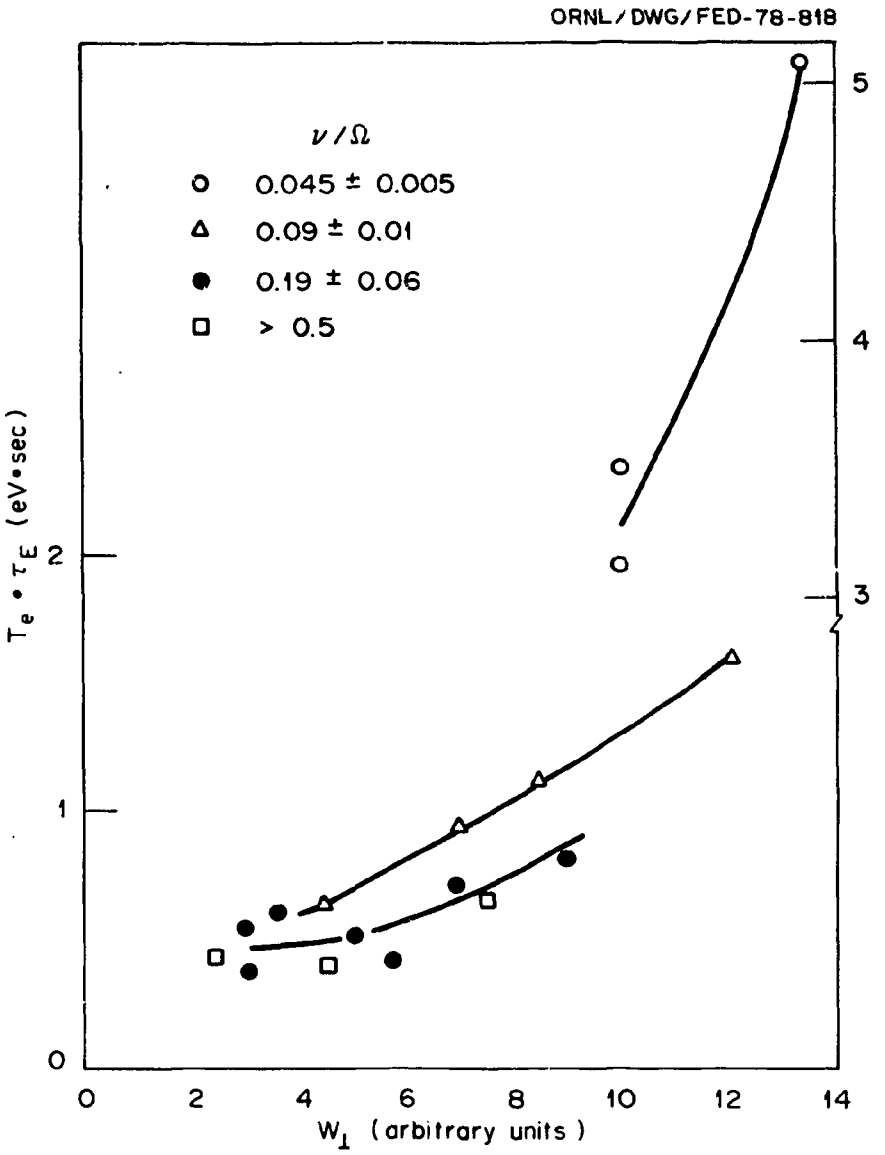

Fig. 12. Normalized energy confinement time plotted against the annularly deposited power with collisionality as a parameter.

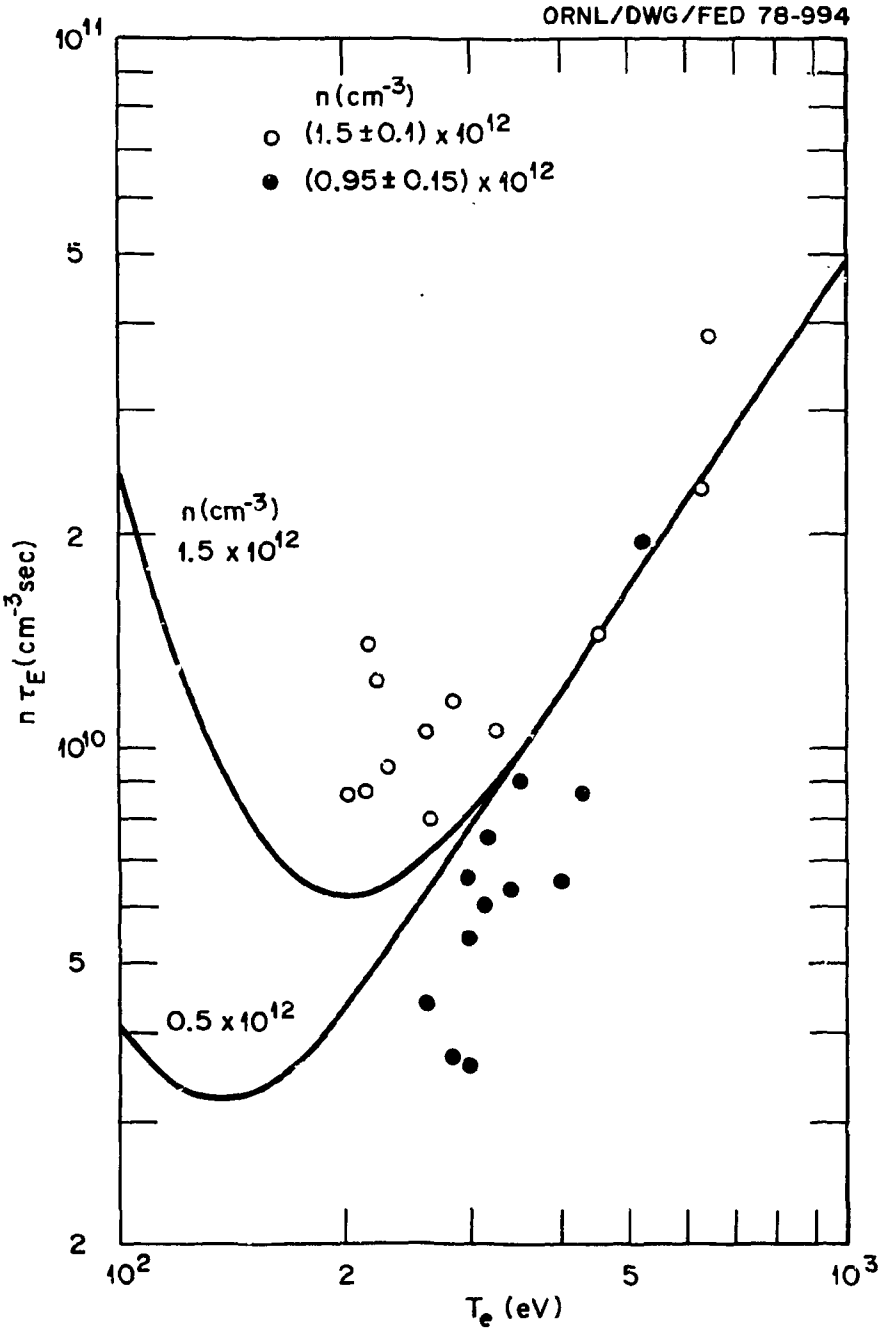

Fig. 13. $n_e\tau_E$ is plotted against T_e with n_e as a parameter. The lines are calculated from Eq. (9), where the constant value is determined for the experimental data of T_e = 455 eV, $n_e\tau_E = 1.43 \times 10^{10}$ (sec cm^{-3}), A = 10, and B = 7 kG.

ORNL/TM-6820
Dist. Category UC-20 f, g

INTERNAL DISTRIBUTION

1. F. W. Baity, Jr.
2. D. B. Batchelor
3. L. A. Berry
4. A. L. Boch
5. F. M. Bieniosek
6. J. D. Callen
7. K. H. Carpenter
8. J. A. Cobble
9. R. J. Colchin
10. R. A. Dory
11-29. H. O. Eason, Jr.
30. J. C. Glowienka
31. G. R. Haste
32. C. L. Hedrick, Jr.
33. E. F. Jaeger
34. J. N. Luton
35. O. B. Morgan, Jr.
36. D. B. Nelson
37. H. Postma
38. M. W. Rosenthal
39. J. Sheffield
40. D. A. Spong
41. N. A. Uckan
42. T. Uckan
43. T. L. White
44-46. Laboratory Records Department
47. Laboratory Records, ORNL-RC
48. Fusion Energy Division Communications Center
49. Document Reference Section
50-51. Central Research Library
52-53. Fusion Energy Division Library
54. ORNL Patent Office

EXTERNAL DISTRIBUTION

55. D. J. Anthony, Energy Systems and Technology Division, General Electric Company, 1 River Road, Bldg. 23, Room 290, Schenectady, NY 12345
56. C. Baker, Fusion Engineering Department, General Atomic Company, P. O. Box 81608, San Diego, CA 92138
57. J. W. Beal, Office of Confinement Systems, Office of Fusion Energy, G-234, Department of Energy, Washington, DC 20545
58. J. F. Clarke, Office of Fusion Energy, G-234, Department of Energy, Washington, DC 20545
59. P. L. Colestock, Princeton Plasma Physics Laboratory, P.O. Box 451, C-Site, Princeton, NJ 08540
60. R. W. Conn, Fusion Technology Program, Nuclear Engineering Department, University of Wisconsin, Madison, WI 53706
61. T. Consoli, Centre d'Etudes Nucléaires de Grenoble, B.P. 85 Centre de Tri, 38041 Grenoble Cedex, Grenoble, France
62. F. L. Culler, Electric Power Research Institute, 3412 Hillview Avenue, P.O. Box 10412, Palo Alto, CA 94304
63. R. A. Dandl, 1122 Calle de Los Serranos, San Marcos, CA 92069
64. R. C. Davidson, Applied Plasma Physics Branch, Office of Fusion Energy, G-234, Department of Energy, Washington, DC 20545
65. O. Dean, Office of Confinement Systems, Office of Fusion Energy, G-234, Department of Energy, Washington, DC 20545
66. J. F. Decker, Applied Plasma Physics Branch, Office of Fusion Energy, G-234, Department of Energy, Washington, DC 20545

67. D. A. Dingee, Manager, Fusion Program, Battelle-Northwest, Battelle Blvd., Richland, WA 99352
68. W. R. Ellis, Jr., Advanced Fusion Systems Branch, Office of Fusion Energy, G-234, Department of Energy, Washington, DC 20545
69. H. K. Forsen, Exxon Nuclear Company, Inc., 777 106th Avenue, N.E., Bellevue, WA 98004
70. T. K. Fowler, L-382, University of California, Lawrence Livermore Laboratory, P.O. Box 808, Livermore, CA 94550
71. M. Fujiwara, Institute of Plasma Physics, Nagoya University, Nagoya 464, Japan
72. H. P. Furth, Princeton University, Plasma Physics Laboratory, P.O. Box 451, Princeton, NJ 08540
73. R. W. Gould, Department of Applied Physics, California Institute of Technology, Pasadena, CA 91109
74. G. E. Guest, General Atomic Company, P.O. Box 81608, San Diego, CA 92138
75. E. G. Harris, Department of Physics, University of Tennessee, Knoxville, TN 37916
76. M. E. Hesse, Centre d'Etudes Nucléaires de Grenoble, B.P. 85, Centre de Tri, 38041 Grenoble Cedex, Grenoble, France
77. R. L. Hickok, Electrophysics Division, Rensselaer Polytechnic Institute, Troy, NY 12181
78. S. Hiroe, Institute of Plasma Physics, Nagoya University, Nagoya 464, Japan
79. R. L. Hirsch, Science and Technology Department, 1251 Avenue of the Americas, New York, NY 10020
80. R. Huse, Public Service Electric and Gas Company, 80 Park Place, Newark, NJ 07101
81. H. Ikegami, Institute of Plasma Physics, Nagoya University, Nagoya 464, Japan
82. H. R. Jory, Varian Associates, 611 Hansen Way, Palo Alto, CA 94303
83. A. Kadish, Office of Fusion Energy, G-234, Department of Energy, Washington, DC 20545
84. E. E. Kintner, Office of Fusion Energy, G-234, Department of Energy, Washington, DC 20545
85. N. A. Krall, Science Applications, Inc., 1200 Prospect Street, Box 2351, La Jolla, CA 92037
86. S. P. Kuo, Dept. of Electrical Engineering, Polytechnic Institute of New York, 333 Jay Street, Brooklyn, NY 11201
87. N. H. Lazar, TRW Defense & Space Systems, 1 Space Park, Bldg. R-1, Redondo Beach, CA 90278
88. K. G. Moses, Chief, Reactor Engineering Branch, Office of the Assistant Director for Technical Projects, Office of Fusion Energy, G-234, Department of Energy, Washington, DC 20545
89. E. Oktay, Office of Fusion Energy, G-234, Department of Energy, Washington, DC 20545
90. R. E. Price, Office of Fusion Energy, G-234, Department of Energy, Washington, DC 20545
91. B. H. Quon, TRW Defense & Space Systems, 1 Space Park, Bldg. R-1, Rm. 1070, Redondo Beach, CA 90278

92. D. J. Rose, Department of Nuclear Engineering, Massachusetts Institute of Technology, Cambridge, MA 02139
93. H. S. Staten, Engineering Design and Component Development Branch, D and T Program, Office of Fusion Energy, G-234, Department of Energy, Washington, DC 20545
94. A. Straprans, Varian Associates, 611 Hansen Way, Palo Alto, CA 94303
95. L. D. Stewart, Princeton Plasma Physics Laboratory, P.O. Box 451, Princeton, NJ 08540
96. D. Sweetman, Culham Laboratory, Abingdon, Oxfordshire, England OX14 3DB
97. R. S. Symons, Varian Associates, 611 Hansen Way, Palo Alto, CA 94303
98. J. M. Williams, Office of Fusion Energy, G-234, Department of Energy, Washington, DC 20545
99. H. H. Woodson, Department of Electrical Engineering, The University of Texas at Austin, Austin, TX 78712
100. Office of Assistant Manager, Energy Research and Development, Department of Energy, Oak Ridge Operations Office, Oak Ridge, TN 37830

101-357. Given distribution as shown in TID-4500, Magnetic Fusion Energy (Distribution Category UC-20 f, g, Experimental Plasma Physics and Theoretical Plasma Physics)